

# OVERVIEW OF THE ESSnuSB ACCUMULATOR RING

M. Olvegård, T. Ekelöf, Uppsala University, Sweden  
 E. Benedetto, M. Cieslak-Kowalska, M. Martini, H. Schönauer, E. Wildner  
 CERN, Geneva, Switzerland

## Abstract

The European Spallation Source (ESS) is a research center based on the world's most powerful proton driver, 2.0 GeV, 5 MW on target, currently under construction in Lund. With an increased pulse frequency, the ESS linac could deliver additional beam pulses to a neutrino target, thus giving an excellent opportunity to produce a high-performance ESS neutrino Super-Beam (ESSnuSB). The focusing system surrounding the neutrino target requires short pulses. An accumulator ring and acceleration of an  $H^-$  beam in the linac for charge-exchange injection into the accumulator could provide such short pulses. In this paper we present an overview of the work with optimizing the accumulator design and the challenges of injecting and storing  $1.1 \cdot 10^{15}$  protons per pulse from the linac. In particular, particle tracking simulations with space charge will be described.

## INTRODUCTION

Starting in a few years, the European Spallation Source (ESS) [1] in Lund, Sweden, will provide users with high-flux spallation neutrons for a large variety of experiments where neutrons are needed as a probe. The neutron production is based on a superconducting high-power proton linac which generates a 2 GeV proton beam with 5 MW average power on target. See Table 1 for a selection of the beam parameters at the end of the ESS linac. This impressively powerful proton driver has drawn the attention of particle physics. In particular, the ESS neutrino Super Beam (ESSnuSB) project plans to use a 5 MW beam from the ESS linac to produce an intense neutrino beam in a dedicated target station [2, 3]. The neutrino super beam will be sent in the direction of Garpenberg, Sweden, 540 km from Lund, where a 0.5 Megaton Water Cherenkov detector is located in an underground mine to detect them. Along the propagation to Garpenberg the neutrinos in the super beam, which consists purely of either muon neutrinos or muon antineutrinos, will oscillate to different flavor states and might thus be detected as muon or electron neutrinos in the Cherenkov detector. The flux of electron and muon neutrinos and antineutrinos will be detected with the aim of discovering and measuring leptonic charge-parity (CP) violation. Leptonic CP violation has been long foreseen and ESSnuSB has a high sensitivity to measure it due to the optimal positioning of the detector at the second oscillation maximum [3].

In order for the experiment to be completed within the planned 10 years of operation, ESSnuSB need the high beam intensity to be preserved all the way from the linac to the target. Firstly, the pulse repetition frequency of the linac must be increased such that the nominal duty factor

Table 1: Nominal Beam Parameters at the End of the ESS Linac

Beam energy	2.0	GeV
Pulse beam current	62.5	mA
Pulse duration	2.86	ms
Pulse repetition rate	14	Hz
Beam power	5	MW

of 4% is doubled. In this way 5 MW would be dedicated to the neutron production and another 5 MW to the neutrino generation. Furthermore, the neutrino target station is equipped with a magnetic focusing device, a van der Meer horn, which focuses the secondary pions that are generated as the protons from the ESS hits the target. The horn focuses pions of one sign and defocuses pions of the opposite sign. The sign of the pions to be focused is changed by reversing the direction of the current in the magnet coil. The pions decay predominantly into a muon and a muon neutrino. The former is absorbed before it has time to decay further whereas the latter continues to travel through the earth towards Garpenberg. The neutrino flux at the detector can be optimized by tuning the focusing of the secondary pions. The positively charge pions produce neutrinos and the negatively charged pions produce antineutrinos.

The horn consists of a toroidal magnet where the particle must cross the current conductor to reach the magnetic field region. Roughly 350 kA is needed to generate the necessary field, a current which leads to ohmic heating of the surface [4]. This means that the horn cannot be powered during the 2.86 ms of the duration of the ESS linac pulse. The pulse must be reduced to a few microseconds, while preserving the total beam power delivered to the target. An accumulator ring placed at the end of the linac has been designed for this pulse compression. There, the long pulses from the ESS linac will be transformed into shorter pulses of 1.32  $\mu$ s duration, with a correspondingly increased pulse current. A schematic of the implantation of the ESSnuSB accumulator ring and target station is shown in Fig. 1.

Each pulse from the ESS linac contains  $1.1 \cdot 10^{15}$  protons. The filling of the ring with this very high charge can only be done through injection painting with charge exchange. That means that  $H^-$  ions are accelerated in the linac and transferred to the ring. At the injection point the ions are stripped off their two electrons using a foil, or possibly in the future with laser stripping. This implies that the linac will have to operate alternately with protons and  $H^-$ . The modifications to the linac required for neutrino production have been investigated thoroughly, see [5] for details.

There are several beam pulse configurations available for simultaneous production of neutrons and neutrinos, all of

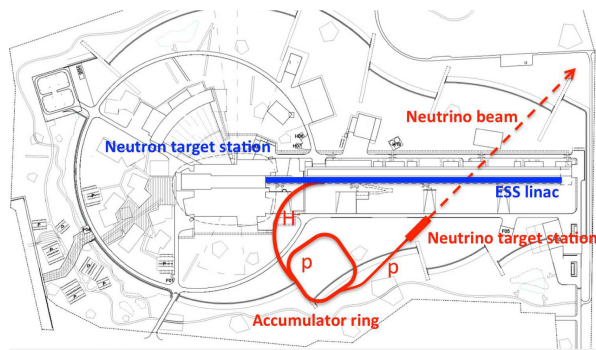


Figure 1: The ESSnuSB implantation at the ESS site.

them resulting in a doubling of the linac duty factor to 8 %. A first option is to simply double the pulse repetition rate from 14 Hz to 28 Hz, making every second pulse an  $H^-$  pulse intended for neutrino production. This option, which is depicted in upper half of Fig. 2, would require a ring with very large aperture or two to four rings stacked on top of each other, similarly to the Proton Synchrotron Booster (PSB) at CERN [6]. Alternatively, the 2.86 ms pulse could be split into two to four batches that would be accumulated separately. That would require pulsing the linac up to 70 Hz, as in the lower part of Fig. 2. Our current baseline option is to split the ESS linac pulse into four such batches, which implies that the accumulator will collect  $2.75 \cdot 10^{14}$  protons for each batch. The simulations presented here assumes this beam intensity and configuration. Later on, other options will be considered.

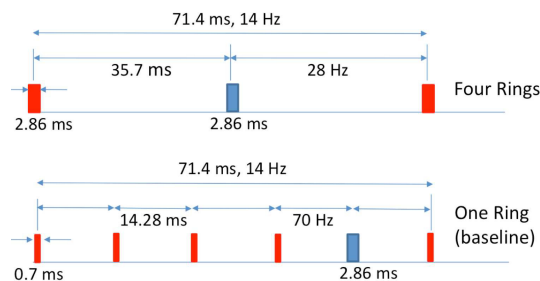


Figure 2: Sketch of the different accumulation scenarios. Protons pulses are in blue and  $H^-$  pulses are in red.

## THE ACCUMULATOR RING

The first version of the lattice of the ESSnuSB accumulator ring was adopted from the similar Spallation Neutron Source (SNS) accumulator ring [7]. The ring was scaled in length to 376 m in order to better suit the higher beam energy of 2.0 GeV, and minor additional adjustments were made. The lattice has a four-fold symmetry with FODO cells in the arcs and four long dispersion-free straight sections for accommodating injection, extraction, RF cavities and instrumentation. The injection region contains a fixed orbit bump and a variable bump with fast kickers. The fast kickers are employed for transverse injection painting.

ISBN 978-3-95450-178-6

The high intensity beam from the ESS linac will suffer tune shifts due to direct space charge. The space charge forces are reduced by painting the transverse phase space in the ring with the linac beam. The  $1\sigma$  normalized transverse emittance of 0.25 mm mrad from the linac will thus be transformed to the target normalized emittance of 100 mm mrad, here covering 86.5% of the beam particles. At the same time, the painting can be modeled to create the desired beam profile. In this case, the interest is to minimize space charge forces and subsequent tune shifts, wherefore it is ideal to have a beam distribution which is as close as possible to uniform in the transverse plane. On the contrary, a Gaussian profile gives rise to space charge forces that are very strong at the density peak, which in turn leads to large tune spreads. We assume a Gaussian beam distribution arriving at the injection point from the linac and aim at modeling the injection painting to produce a quasi square distribution. In addition, heating of the stripping foil due to multiple particle crossings from the circulating beam must be considered in the optimization.

RF cavities, both a first harmonic and a second harmonic cavity, are employed to preserve the extraction gap. The first harmonic is split up over three cavities with in total 5 kV and a second-harmonic cavity in anti-phase of 2.5 kV. Since the accumulation takes only 540 turns and the time between pulses is 14.3 ms the extraction gap cannot be created in the ring but must be generated already in the linac.

An early indication of emittance growth in the vertical plane due to space charge, induced a study of three different working points with a fixed bare tune in the horizontal plane. The working points are as follows:

- $Q_x = 10.395, Q_y = 11.321$
- $Q_x = 10.395, Q_y = 11.254$
- $Q_x = 10.395, Q_y = 11.202$

They will later be referred to by the labels *a*, *b* and *c*.

## SIMULATIONS

We have performed beam tracking simulations using the ESSnuSB accumulator lattice. The tracking has been done using the particle-in-cell code pyORBIT [8], with comparison tests in Accsim [9]. PyORBIT uses PTC [10] external libraries, which is particularly convenient when using time dependent elements, such as the fast kickers for the injection painting. Two sets of simulations were done to study the beam under the effect of space charge. The first set considers the full beam intensity, thus after the injection has been completed. The second includes the injection painting and simulates the full accumulations process. Part of the second set was also compared with an equivalent simulation done in Accsim. The details of these simulations will be described here.

### Full Intensity

In the baseline design, the accumulator ring lattice will have to be able to store a total beam intensity of  $2.75 \cdot 10^{14}$

protons during the time between injection and extraction, possibly for a few hundred turns. A first series of simulations were made to assess whether the current lattice design can do that without losses and with minimal emittance growth. To this end, we used the lattice with injection kickers turned off, i.e. without the fast orbit bump but with the fixed bump. We used the lattice in three configurations corresponding to the three working points *a*, *b* and *c*, always with RF cavities powered. Note that there is no ramping of the cavities since there is no acceleration.

As a worst-case scenario we have assumed a Gaussian beam distribution with a  $1\sigma$  geometrical emittance of 8.5 mm mrad, which corresponds to the target emittance in the ring. In reality we hope to produce a more flat distribution with the injection painting. A Gaussian energy distribution with rms spread 0.02 % was chosen, in agreement with what is expected at the end of the ESS linac. The longitudinal distribution was set to uniform but with a 15 % gap for extraction.

The ring lattice was imported from a MADX file and a file was created which contains all the elements divided into slices. In each slice, or node, a space charge kick is applied. Roughly 500 space charge nodes were used. We include a 2D transverse space charge model with a grid of  $128 \times 128$  bins, which is weighted slice by slice with the longitudinal beam density (“2.5D”) calculated in 128 slices. In addition, we include longitudinal space charge forces with 128 bins. The number of bins in the space charge models, as well as the amount of 100’000 macro-particles used in the tracking, have been selected based on a series of simulations where the computation time is weighed against the accuracy of the convergence of the result.

Figures 3 and 4 show the emittance evolution in the horizontal and the vertical plane during the 500 turns the tracking was performed. The rms emittance growth is plotted relative to the initial value, which reveals the fact that working point *a* exhibits a clear growth in the vertical plane whereas the horizontal emittance has its smallest growth for the same working point. We see some remnant numerical noise, though, a higher number of macro-particles yields the same overall result.

A tune spread of approximately 0.2 is obtained both numerically with pyORBIT and analytically with the Laslett coefficients.

### With Injection Painting

With a revolution period of 1.32  $\mu$ s it takes 540 turns to accumulate one batch, corresponding to a fourth of a nominal proton pulse from the linac. This injection will be done through painting, where the injection point is fixed to 42.5 m in the horizontal direction and 46 mm in the vertical direction with respect to the closed orbit without injection bump. At the start of the injection the bump is at its maximum amplitude around 30 mm, see Fig. 5, and therefore closer to the injection point. During the time it takes to inject one batch, the amplitude is reduced. Only after the injection is complete, the bump amplitude is set to zero.

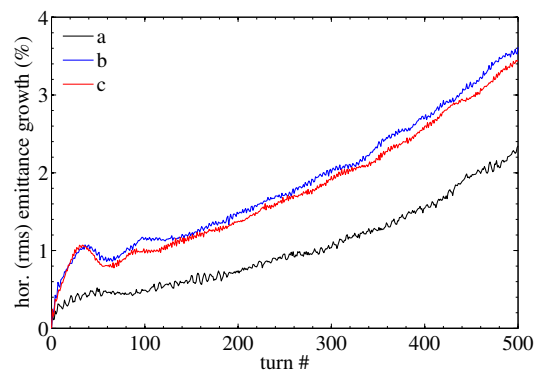


Figure 3: Worst-case scenario: Horizontal emittance growth relative to the initial emittance, plotted for the three working points.

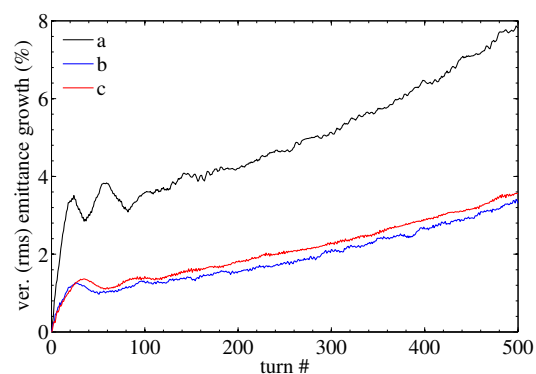


Figure 4: Worst-case scenario: Vertical emittance growth relative to the initial emittance, plotted for the three working points.

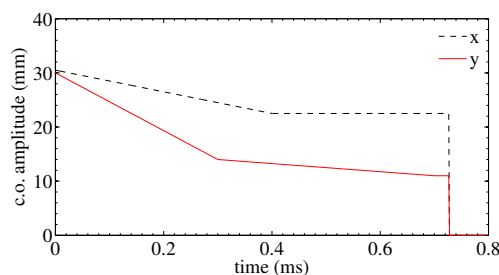


Figure 5: The closed orbit bump (c.o.) amplitude as a function of time. At the end of the injection, at  $t = 0.73$  ms corresponding to 550 injected turns, the bump amplitude is set to zero for computational ease. In reality it takes some microseconds to completely remove the bump.

The same space charge models and binning as in the simulation set described above was used here. This time a beam with Gaussian transverse distribution with emittance corresponding to the ESS linac beam was used. As before, we chose a Gaussian energy distribution with rms spread 0.02 % and uniform longitudinal distribution with a 15 % gap for extraction. We inject one such bunch every turn, represented by 2000 macro-particles, and inject during 550

turns. After the injection is complete we track for another 50 turns and then extract the total particle distribution, now consisting of  $1 \cdot 100'000$  macro-particles.

The emittance evolution during the injection is displayed in Fig. 6. Contrary to the first simulation set, these results indicate that working point *c* is not the best choice for our lattice. Although the emittance growth is small in the horizontal plane it is quite large in the vertical plane in comparison to working points *a* and *b*. By looking at the emittance growth that we would expect without space charge forces, shown in Fig. 7, we conclude that working point *b* seems best from the point of view where effects from space charge forces are minimized.

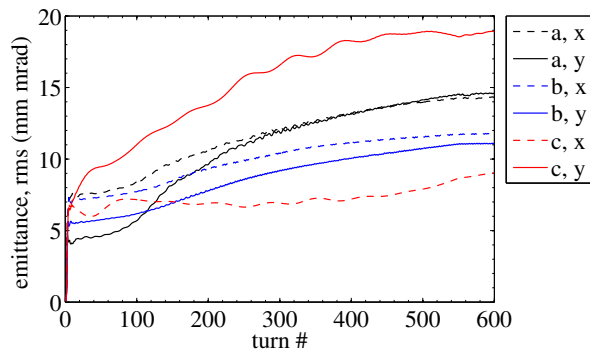


Figure 6: With painting: Horizontal and vertical emittance during injection, plotted for the three working points.

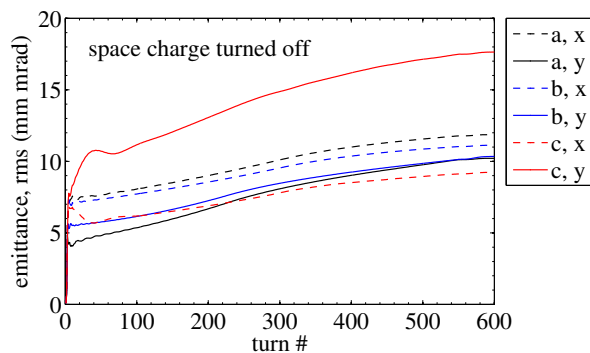


Figure 7: With painting: Emittance evolution for the three working points when space charge forces are ignored.

Taking a closer look at the beam after tracking in lattice in the configuration of working point *b* we see that there is room for further optimization. Figure 8 shows the horizontal and vertical profiles. The profiles are not flat but rather triangular with a hint of halo formation. There is also an asymmetry in the transverse phase space distributions, revealed in the density plots in Fig. 9. Both the asymmetry and the peaked profiles will have to be reduced by remodeling the injection kicker ramp that defines the painting procedure.

Lastly, we show the tune diagram in Fig. 10. The core of the beam hits the fifth order vertical resonance line and the third order horizontal resonance line. The classic neck-tie

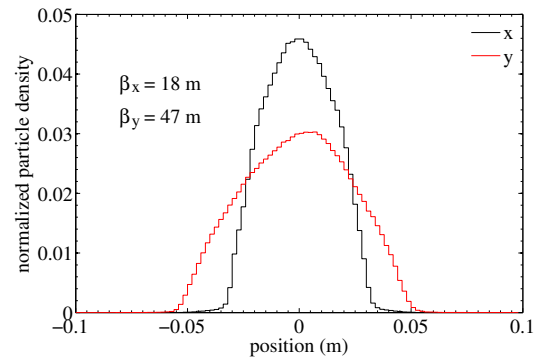


Figure 8: Projections onto the horizontal axis and the vertical axis, working point *b*.

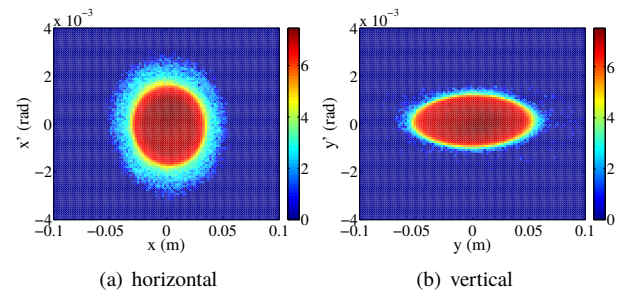


Figure 9: Density plots of the horizontal (a) and vertical (b) phase space. The colorbar marks the density in log scale.

shape is lost which makes it difficult to identify an overall tune shift, though it is below the 0.2 obtained in the simulation set at full intensity. The tune diagrams look similar for the three working points.

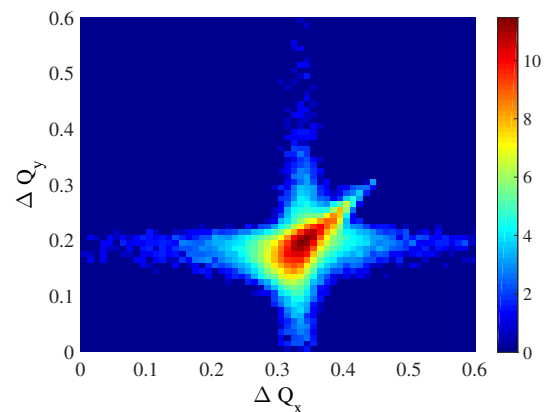


Figure 10: Tune density diagram where the color bar shows the density in log scale.

### Comparison with Accsim

When modeling the injection procedure one must consider that the foil used for stripping the injected  $H^-$  ions cannot sustain unlimited particle crossings by the circulating beam. The simulation program Accsim was used to investigate the number of foil hits, from which the energy

deposition and temperature increase in the foil can be estimated. The thermal response of the foil to the beam has also been investigated analytically [11]. A simulation with Accsim, including the full painting procedure, was done with the lattice configuration  $c$  and similar parameter sets as described above. The result was compared with results from pyORBIT.

The horizontal and the vertical profiles obtained in the two simulations are shown in Fig. 11. While the horizontal profiles agree within the statistical uncertainty, in vertical the pyORBIT simulation result in a notably larger profile. Though the discrepancy is not yet fully understood it is worth mentioning that the number of macro-particles is limited to 99'000 in the case of Accsim. The limited statistics may at least partially account for the asymmetry in the profiles.

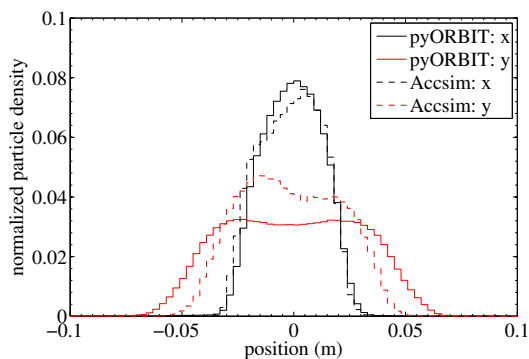
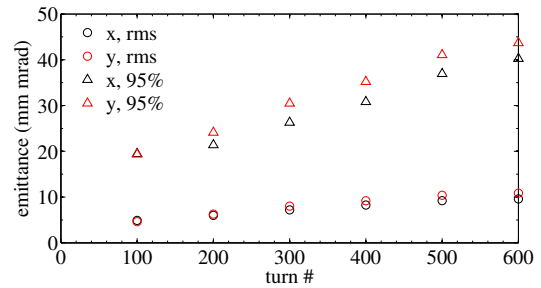


Figure 11: Projections onto the horizontal axis (black) and the vertical axis (red), working point  $c$ . A comparison between pyORBIT (solid line) and Accsim (dashed line).

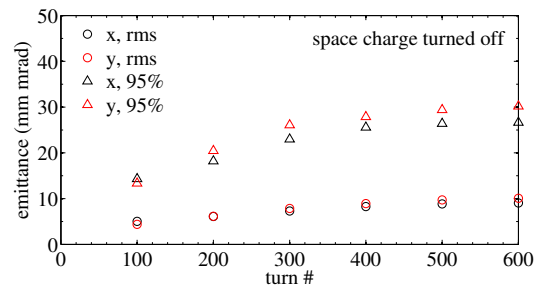
In addition we present the evolution of the rms emittance obtained with Accsim in Fig. 12(a), with space charge turned on, and Fig. 12(b) with space charge turned off, to be compared with Figs. 6 and 7. Also from these plots it becomes apparent that there is a discrepancy in the vertical plane between the two programs. Note, however, that when the result obtained with and without space charge are compared, Accsim exhibits a strong emittance growth in both planes in the 95 % emittance. It is still to be confirmed whether the final emittances obtained in the Accsim and pyORBIT simulations are within the target of 100 mm mrad, normalized (86.5 %).

## CONCLUSION AND OUTLOOK

We have performed beam tracking studies with space charge in order to evaluate the first design of the ESSnuSB accumulator ring. The study includes tracking at full intensity in order to assess the severity of the space charge effects and associated tune shifts that are to be expected. In addition, simulations including the phase space painting have been made. The result indicates that the painting procedure require further optimization. The next step is therefore to look into various transverse painting schemes. The lattice may be re-tuned to move away from dangerous resonances.



(a) space charge ON



(b) space charge OFF

Figure 12: Emittance evolution during injection obtained with Accsim when space charge is turned on (a) and off (b) in the simulation.

The beam arriving from the ESS linac will consist of trains of micro bunches. The bunches are 3 ps long and are bunched at 352 MHz. Future studies will investigate the effect of the micro-bunching on the beam behavior in the ring.

## REFERENCES

- [1] S. Peggs (Ed.), ESS Technical Design Report, 2013.
- [2] E. Baussan *et al.*, *Nucl. Phys. B*, vol. 885, pp. 127-149, 2014.
- [3] E. Wildner *et al.*, accepted for publication in *Advances in High Energy Physics*, Hindawi publishing, 2016. <http://arxiv.org/abs/1510.00493>
- [4] N. Vassilopoulos, "The ESS neutrino super beam optimization design studies", NuFact workshop, Beijing, China, 2013.
- [5] F. Gerigk and E. Montesinos, "Required modifications of the ESS accelerator architecture for ESSnuSB", CERN-ACC-NOTE-2016-0XXX (2016).
- [6] K. Reich, "The CERN Proton Synchrotron Booster", in *Proc. of PAC'69*, pp. 959-961, 1969.
- [7] W. T. Weng, BNL-65618, 1998.
- [8] A. Shishlo *et al.*, *Procedia Computer Science* 51, pp. 1272, 2015.
- [9] F. W. Jones *et al.*, *Part. Accel.* 31, pp. 199-204, 1990.
- [10] E. Forest *et al.*, CERN-SL-2002-044 (AP), KEK-Report 2002-3, 2002.
- [11] M. Martini, CERN-ACC-NOTE-2015-0005, 2015.